EARTH SURFACE PROCESSES AND LANDFORMS
Earth Surf. Process. Landforms (2019)

Published online in Wiley Online Library
(wileyonlinelibrary.com) DOI: 10.1002/esp.4572

Estimating sand concentrations using ADCP-based acoustic inversion in a large fluvial system characterized by bi-modal suspended-sediment distributions

Ricardo N. Szupiany,[1,2]* Cecilia Lopez Weibel,[1,2] Massimo Guerrero,[3] Francisco Latosinski,[1,2] Molly Wood,[4] Lucas Dominguez Ruben[1,2] and Kevin Oberg[5]

[1] International Center for Large Rivers Research, School of Engineering and Water Sciences, Universidad Nacional del Litoral, Santa Fe City, Argentina
[2] National Scientific and Technical Research Council (CONICET), (C1033AAJ) CABA, Buenos Aires, Argentina
[3] Hydraulic Engineering Laboratory, University of Bologna, Bologna, Italy
[4] US Geological Survey, Boise, ID USA
[5] US Geological Survey, Urbana, IL USA

Received 24 November 2017; Revised 6 December 2018; Accepted 17 December 2018

*Correspondence to: Ricardo N. Szupiany, International Center for Large Rivers Research (CIEGRi), Faculty of Engineering and Water Sciences, Universidad Nacional del Litoral, Ciudad Universitaria RN 168 (3000), Santa Fe, Argentina. E-mail: rszupian@fich.unl.edu.ar

ESPL
Earth Surface Processes and Landforms

ABSTRACT: Quantifying sediment flux within rivers is a challenge for many disciplines due, mainly, to difficulties inherent to traditional sediment sampling methods. These methods are operationally complex, high cost, and high risk. Additionally, the resulting data provide a low spatial and temporal resolution estimate of the total sediment flux, which has impeded advances in the understanding of the hydro-geomorphic characteristics of rivers. Acoustic technologies have been recognized as a leading tool for increasing the resolution of sediment data by relating their echo intensity level measurements to suspended sediment. Further effort is required to robustly test and develop these techniques across a wide range of conditions found in natural river systems. This article aims to evaluate the application of acoustic inversion techniques using commercially available, down-looking acoustic Doppler current profilers (ADCPs) in quantifying suspended sediment in a large sand bed river with varying bi-modal particle size distributions, wash load and suspended-sand ratios, and water stages. To achieve this objective, suspended sediment was physically sampled along the Paraná River, Argentina, under various hydro-sedimentological regimes. Two ADCPs emitting different sound frequencies were used to simultaneously profile echo intensity level within the water column. Using the sonar equation, calibrations were determined between suspended-sand concentrations and acoustic backscatter to solve the inverse problem. The study also analyzed the roles played by each term of the sonar equation, such as ADCP frequency, power supply, instrument constants, and particle size distributions typically found in sand bed rivers, on sediment attenuation and backscatter. Calibrations were successfully developed between corrected backscatter and suspended-sand concentrations for all sites and ADCP frequencies, resulting in mean suspended-sand concentration estimates within about 40% of the mean sampled concentrations. Noise values, calculated using the sonar equation and sediment sample characteristics, were fairly constant across evaluations, suggesting that they could be applied to other sand bed rivers. © 2018 John Wiley & Sons, Ltd.

KEYWORDS: ADCP; echo intensity level; suspended sediment; bi-modal particle size distribution; sand bed rivers

Introduction

Traditional methods often used to estimate suspended-sediment transport rates require the deployment of appropriate sediment samplers (Davis, 2005) and, if sampling from a boat, holding the boat stationary for water column sediment sampling (Gray *et al.*, 2008). The water flow variable for calculating sediment flux often is determined through stationary or moving-boat acoustic Doppler current profiler (ADCP) measurements (Turnipseed and Sauer, 2010; Mueller *et al.*, 2014). These discrete sediment sampling and flow measurement methods, traditionally used together to estimate sediment flux, have been widely evaluated and accepted; however, the total cost associated with field measurements can be substantial or even prohibitive (Gray *et al.*, 2008), especially in rivers that cannot be waded. Moreover, safety considerations during floods or periods of heavy navigational traffic sometimes prevent collecting samples.

Additionally, and maybe the most important factor for the geomorphological and sediment research community, the low space–time resolution achieved by these methods hinders the understanding of the interaction of flow and sediment transport and resulting morphodynamics on river systems.

During the last two decades, a variety of surrogate technologies based on optical, laser, and acoustic principles has been proposed to address these technological, economic, and safety issue shortcomings (Gray and Gartner, 2010). Though successful application of surrogate technologies to quantify sediment transport rely on the collection of suspended-sediment samples to develop calibrations (Gray and Gartner, 2010), these calibrations can be applied when it is not feasible to collect samples, ultimately reducing the cost and risk of obtaining sediment data. Acoustic technologies, based on commercial ADCPs, have been recognized as potential tools for the quantification of sediment transport in natural streams using their echo intensity levels as a measure of acoustic backscattering strength. The use of ADCPs present some important advantages in comparison with the other technologies such as the possibility to simultaneously measure flow and backscatter strength, with high spatial and temporal resolution, while moving the ADCP across the river.

Research has focused (using down-, side- or up-looking ADCP deployment) on the relation of suspended sediment and corrected backscatter (Thorne *et al.*, 1993, 1998; Reichel and Nachtnebel, 1994; Holdaway *et al.*, 1999; Thorne and Hanes, 2002; Gartner, 2004; Wall *et al.*, 2006; Topping *et al.*, 2007; Deines, 1999; Szupiany *et al.*, 2009; Hanes, 2012; Guerrero *et al.*, 2013, 2016; Latosinski *et al.*, 2014; Thorne and Hurther, 2014; Landers *et al.*, 2016; Manaster *et al.*, 2016; Venditti *et al.*, 2016; Topping and Wright, 2016; Mullison, 2017; Hackney *et al.*, 2018), acoustic attenuation and scattering properties (Thorne and Meral, 2008; Wright, *et al.*, 2010; Sassi *et al.*, 2012; Moate and Thorne, 2013; Moore *et al.*, 2013; Agrawal and Hanes, 2015; Hanes, 2016; Topping and Wright, 2016; Haught *et al.*, 2017), and acoustic scattering by suspended flocculating sediments (Thorne and Hurther, 2014; Vincent and McDonald, 2015; Thomas *et al.*, 2017).

Despite this progress, further effort and evaluation are required, especially over a range of natural conditions and in sand bed rivers characterized by sediment transport mixtures that include both suspended river bed sand and finer (wash load) fractions of silt and clays. At most river sites, fine wash-load fractions of sediment are homogeneously distributed across a river cross-section, but sand-sized fractions of sediment can greatly vary with depth and width. Moreover, both wash load and sand fractions may vary by site and hydrologic condition, altering the characteristics of sound propagation into sediment-water mixture and resulting measurements of echo intensity level (acoustic backscatter) and attenuation (Wright *et al.*, 2010; Agrawal and Hanes, 2015; Hanes, 2016). The importance of acoustic backscatter and attenuation of suspended sediment has received a fair amount of attention during the past few years; nonetheless, many theoretical formulations and simplifications remain invalid or untested in field environments when sediment characteristics substantially vary within an acoustic measurement volume, which hinders the development of a more general methodology to be applied by using down-looking ADCPs.

The objective of this article is to investigate the behavior of sound propagation produced by ADCPs in a large river with bimodal particle size distribution (PSD), which is typical of sediment characteristics of many rivers throughout the world. Field surveys were conducted in conditions with different ratios between suspended wash-load (clay–silt) concentration (M_{s1}) and sand concentration (M_{s2}), at various sites and water stages. For each study condition, each term of the sonar equation is analyzed with focus on: (i) the noise level variation, (ii) effect of PSDs and M_{s1}/M_{s2} ratios on sound attenuation and backscattering strengths, (iii) influence of ADCP powering source and, (iv) ADCP-emitted sound frequency. Finally, scope, limitations and recommendations of the applied methodology are discussed to propose good practices for similar applications in sand bed rivers.

Study Area and Methodology

Two zones were surveyed multiple times on the Paraná River, Argentina (Figure 1). The first study area (Zone A), located close to Santa Fe City, Argentina (31°39′17.04″S, 60°35′33.87″W) is on the Colastiné River, which is a secondary channel of the Paraná River middle reach (see Figure 1b). The second surveyed area (Zone B) is at the main channel of the Paraná River on a reach upstream from Zone A, slightly downstream of the confluence with the Paraguay River (27°22′23.41″S, 58°43′7.18″W) (see Figure 1a). Fieldwork was conducted under two hydrologic conditions at Zone A, on March 17, 2014 and September 20, 2014 (referred in text as surveys Aa and Ab, respectively) and on February 25, 2015 at Zone B. The discharges in the Colastiné River at the time of the surveys were 1485 $m^3 s^{-1}$ and 1983 $m^3 s^{-1}$ for Aa and Ab, respectively, with the first survey corresponding to a mean annual flow level and the second survey at a bankfull stage. For Zone B, the discharge was 16 659 $m^3 s^{-1}$ during the experimental campaign, corresponding to a low level (mean annual flow of 19 537 $m^3 s^{-1}$).

In the upper reach (Zone B) downstream of the Paraná–Paraguay confluence, a substantial amount of silt, clay and very fine sand inflow from the Bermejo–Paraguay Rivers is expected from January to April with a typical total concentration range of 1000 to 2000 mg l^{-1} (Drago and Amsler, 1988; Lane *et al.*, 2008). Upstream of the confluence, the Paraná River usually transports very low suspended-sediment concentrations (i.e. less than 30 mg l^{-1}), as observed in different colors upstream and downstream of the confluence (Figure 1a). At its middle reach (Zone A), silt- and clay-size sediment are homogenously distributed without substantial variation within the water column and cross-section (Drago and Amsler, 1988, 1998; Lane *et al.*, 2008). For this study, sediment particle sizes larger than or equal to 62.5 μm were considered to be the sand (coarse) fraction; smaller particles were considered to be the wash load (fine clay–silt) fraction.

At the study zones, the bed is composed almost completely of sand (> 90%) with small amounts of silt and clay (< 4%) (Drago and Amsler, 1998). Drago and Amsler (1998) reported the presence of coarse and medium sand (mean particle size of 412 mm) within the range 28–63% in bed material samples at Zone B, whereas these percentages decrease markedly to 11% and 51% and mean particle size reduces to 320 mm in bed material samples in Zone A.

In contrast with available bed material PSD information, the characteristics of suspended sediments have not been well described by previous studies. Recently, Latosinski *et al.* (2014) observed, at Zone A, mean particle with sizes of 105 μm and 7 μm for the suspended-sand and clay–silt fractions, respectively.

Fieldwork consisted of simultaneous water column profiling using two Rio Grande ADCPs from Teledyne RD Instruments that operated at 1200 kHz and 600 kHz frequencies. These provided vertical profiles of flow velocity and water column echo intensity. In parallel, isokinetic suspended-sediment samples were taken by means of a US P-61 point sampler (Edwards and Glysson, 1999; Davis, 2005) using an US Geological Survey (USGS) E-reel. These measurements were performed from an anchored boat during optimal weather conditions, which limited the overall motion (heave, yaw and pitch) and any lateral drifting on the anchor to less than 2 m during the sampling periods. The sampler's hydraulic efficiency was tested at the

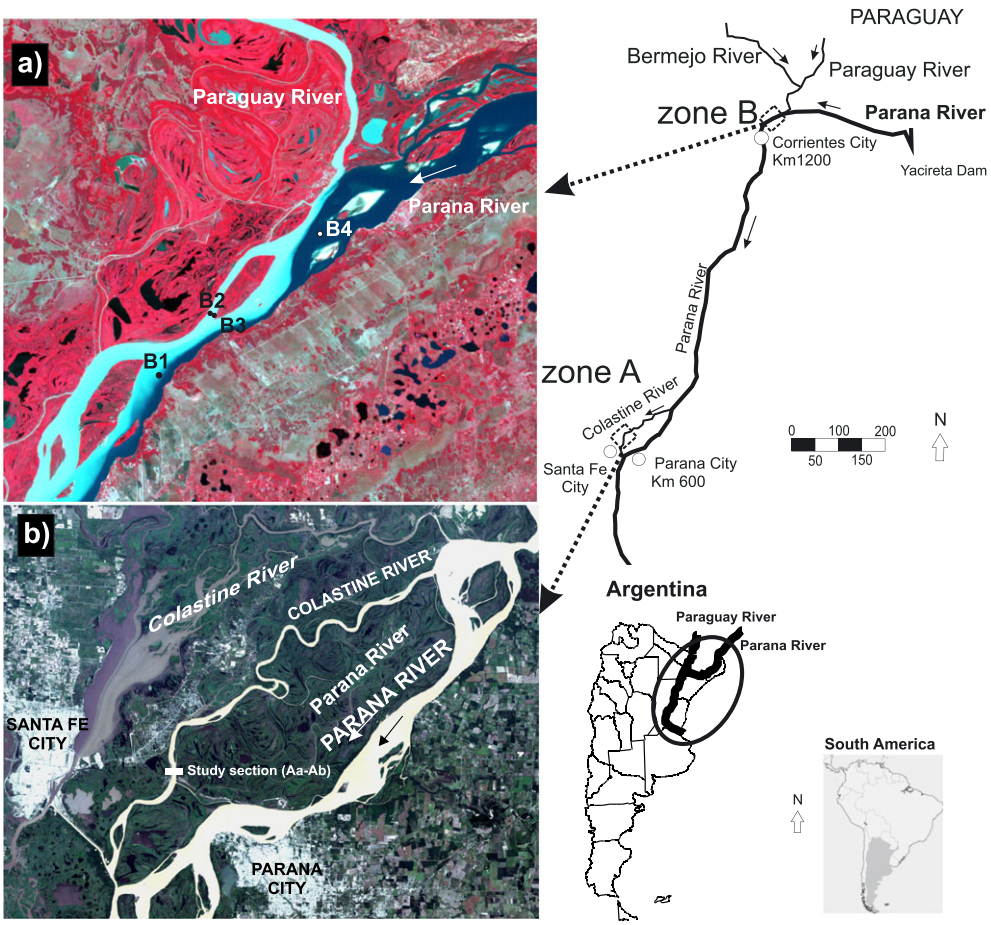

Figure 1. Study zones. (a) Zone B: Upper Paraná reach downstream of the Paraná–Paraguay confluence. (b) Zone A: Middle Paraná reach and its secondary reach Colastiné River. Note in Zone B the sampled verticals (B1–B4) are located downstream of the Paraná–Paraguay confluence. [Colour figure can be viewed at wileyonlinelibrary.com]

beginning of each survey, eventually setting the period for opening and closing of the nozzle to produce isokinetic sampling. During the first survey Aa (Colastiné River), both ADCPs were used, whereas only the 1200 kHz instrument was deployed in survey Ab and Zone B.

The same fully charged battery was used to power both ADCPs in survey Aa. A brand new fully charged battery and a generator with a power inverter were used in survey Ab and Zone B, respectively.

A differential global positioning system (DGPS) with real-time kinematic (RTK) correction was used to continuously and accurately record the boat and instrument position and velocity.

In the first survey (Aa), five verticals (namely Aa1, Aa2, Aa3, Aa4 and Aa5) were investigated across the river channel. The Equal Discharge Increment (EDI) method (Edwards and Glysson, 1999) was used to determine the locations of the sampling verticals, using ADCP cross-section measurements processed in software developed by the USGS (http://hydroacoustics.usgs.gov/movingboat/EDI1.shtml). To increase the amount of data for evaluation, additional verticals Aa6 and Aa7 were located between Aa3–Aa4 and Aa4–Aa5, respectively.

The second survey Ab, consisted of three verticals (Ab1, Ab2 and Ab3) located at different positions along the study reach, which gave different hydraulic and sediment transport conditions.

In Zone B, four verticals (B1, B2, B3 and B4, see Figure 1a) across the river channel measured different conditions of suspended material from the Paraná and Paraguay Rivers, according to the sediment distribution downstream of the confluence. Verticals B2 and B3 were at the right side of the channel where the highest concentrations were expected because of the Paraguay River inflow; B1 was located in the mixing region of the confluence and B4 was at the true left side of the channel, outside of the turbidity plume produced by the Paraguay River inflow.

Five samples per vertical, corresponding to 0.2, 0.4, 0.6, 0.8 and 0.9 of the water depth (h), were collected in survey Aa and Zone B while three depths were sampled at survey Ab (0.2, 0.6 and 0.8 h). ADCPs concurrently profiled flow velocity and water column echo intensity.

Wet sieving, water evaporation, sediment drying, and weighing were performed for each sample to segregate wash load and sand fractions of sediment concentrations in the sampled volume. These techniques provided wash-load concentration (M_{s1}) and suspended-sand concentration (M_{s2}) values, respectively, and were used later for particle size analysis.

For Zone A, the wash-load material was analyzed by using the particle sizing Malvern Mastersizer 2000. Three repetitions were averaged for each sample. ImageJ code processing (Rasband and Ferreira, 2012) and a scanning electron microscope (SEM) were applied to analyze the sand fractions according to methods in Kumar *et al.* (2010). The Horiba LA-910 Particle Size Analyzer measured the mean particle sizes of both sand and wash-load fractions of samples from Zone B. Volumetric particle distribution obtained from both methods was transformed to number particle distribution following Moore *et al.* (2013). The number particle distribution was used for all analyses. Note that samples from verticals Aa6, Aa7, Ab1, Ab2 and Ab3 were not fully processed for all particle size parameters; the concentration values from these samples were

used to validate the acoustic methodology assuming the mean particle sizes from survey Aa.

ADCP and Suspended Sediment: A Review of Theoretical Considerations

+B: Acoustic formulation for suspended-sediment particles

The propagation of an emitted signal with power intensity I_0 (EL in dB with an arbitrary reference intensity I_{ref}) into a water sediment mixture is usually modeled accounting for the volume backscatter strength (S_v), sound losses and spherical spreading, which may be referred to as volume backscatter correction (S_c in dB) eventually giving the received power intensity I (referred to as RL in dB with the same arbitrary reference intensity I_{ref} as for EL). Under ideal conditions, the received intensity is proportional to the emitted level and the corrected backscatter strength (i.e. $S_v - S_c$ in dB). Therefore, a simple equality may be written in dB scale as given in Equations (1) and (2).

$$\mathrm{EL} + S_v - S_c = \mathrm{RL} \tag{1}$$

$$10\log^{10}\left(\frac{I_0}{I_{ref}}\right) + S_v - S_c = 10\log^{10}\left(\frac{I}{I_{ref}}\right) \tag{2}$$

The presence of a cloud of suspended particles rather than a single particle implies the use of the S_v, which is simply defined as the sum of the backscattering cross-sections of suspended particles in a unit volume. In addition, the average properties of the scattering particles may be considered for practical issues as expressed in Equation (3) (Thevenot and Kraus, 1993):

$$S_v = 10\log_{10} n_b \sigma_s \tag{3}$$

where the mean expected values are denoted between brackets $\langle\rangle$, therefore, in Equation (3), $\langle\sigma_s\rangle$ is the average backscattering cross-section (in m^2), while, n_b is the number of scatterers per unit volume (in m^{-3}).

In any case, the scattering cross-section is related to the physical cross-section of an individual particle by means of the scattering function. This relation for a sphere in the omnidirectional scatter regime may be written as follows (Clay and Medwin, 1977):

$$\sigma_s = \left(a^2 \cdot f^2\right)/4 \tag{4}$$

where f refers to the form factor and a to particle radius.

For a given particle radius, the form factor depends on the applied sound frequency; for changing particle radius, its variation is described with the wavenumber-particle radius product x (where $x = kax = ka_s$ and k is the wavenumber).

When referring to a cloud of irregularly shaped particles, such as in the case of suspended sediment in natural rivers, the formulation presented by Thorne and Meral (2008) may be applied to estimate f as: $f = 1.25 \times^2$ and $f = 1.1$ for Rayleigh ($x < 1$) and geometric ($x >> 1$) scattering regimes, respectively. Note that at Rayleigh regime, the wavelength of the sound is much greater than the particle circumference and scattering is considered to be independent of the shape of the scatterer (Thorne and Meral, 2008).

Considering the total mass of suspended sediments per unit volume, M_s, equals to the sum of n_b equivalent spheres characterized with the average radius $\langle a\rangle$ and density ρ_s,

$$M_s = \frac{4}{3}\pi\rho_s n_b a^3, \tag{5}$$

where the angular brackets denote the operation.

$$g = \int_0^\infty g(a)\, n(a)\, da\, g = \int_0^\infty g(a) n(a) da \tag{6}$$

where $n(a)$ represents the size distribution of particles in suspension and $g(a)$ represents any function of the particle size (Sassi *et al.*, 2012).

Relation between volume backscatter strength and suspended-sediment mass in the unit volume follows:

$$S_v = 10\log_{10}\frac{3M_s\sigma_s}{4\pi\rho_s a^3} \tag{7}$$

Combining Equations (4), (5) and (7), the volume backscatter strength, S_v, may be conveniently written as:

$$S_v = 10\log_{10}(K_{s1}M_{s1} + K_{s2}M_{s2}) \tag{8}$$

where K_{si} is a function of time t and the ranging distance along the central axis of the beam, R,

$$K_{si}(t,R) = \frac{3{a_i}^2{f_i}^2}{16\pi\rho_s {a_i}^3} \tag{9}$$

To account for bimodal distribution of the particle size, subscripts 1 and 2 represent wash load and suspended-sand sediment fractions, respectively.

Given the model of backscatter (Equations (8) and (9)), the level of echo intensity recorded by an ADCP in counts may be applied to characterize the scattering particles in terms of concentration and particle size (i.e. inverse problem solution) or to calibrate the instrument parameters that affect the measured levels by using reference values of concentration and particle size from samples (i.e. the direct problem approach), as observed in this study.

The volume backscatter correction, S_c, is expressed by means of: (i) the absorption coefficient due to water viscosity, α_W, that may be expressed in dB m^{-1} following Schulkin and Marsh (1962), among others, (ii) the absorption coefficient, α_S, due to sediment scattering out of the acoustic beam (i.e. scattering attenuation, α_{SS}) and the friction between sediment particles and water (i.e. viscous attenuation, α_{SV}), that is computed in dB m^{-1} considering formulation by Urick (1983) and Thorne and Hanes (2002), and (iii) beam spreading and near-field zone correction by means of the coefficient ψ as suggested by Downing *et al.* (1995).

Following the same criteria as for S_v, α_S may be subdivided into contributions from wash load and suspended-sand sediment fractions. Therefore, the total backscatter correction S_c is expressed by:

$$\begin{aligned} S_c = {} & 2(\alpha_w + \alpha_{sv1} + \alpha_{sv2} + \alpha_{ss1} + \alpha_{ss2})R \\ & + 10\log_{10}\left(T_t R^2 \psi^2\right) \end{aligned} \tag{10}$$

where T_t $T_t$is the water temperature.

A variety of expressions equivalent to Equations (1) and (2) can be found in the literature depending on the use of dB or exponential forms with their reference values, applied coefficients to summarize instrumental and scattering properties, and on operational simplifications. Given that the ADCP gives an indicator of the received intensity level in a logarithmic scale, ADCP users may prefer a dB expression, such as Equation (2)

with RL proportional to the ADCP recording in counts. For this reason, the sound attenuation in Equation (10) is expressed in dB m^{-1}, rather than using the natural exponential function by Thorne and Hanes (2002).

Overall acoustic reverberation measured with an ADCP

A variety of sources might produce underwater sound reverberation (e.g. scatter from air bubbles, flocculating matter, particulate organic matter) rather than silt, clay and sand particles. In fact, a basic concept is that the echo intensity level (E) may be divided into desired and undesired portions of the received signal (commonly referred to as noise or background masking level). A variety of masking effects may distort the information contained in the received signal regarding suspended sediment or a specific particle size. Indeed, the ADCP recording in counts, E, represents both portions of the received signal as reported in Equation (11) (Deines, 1999) and Equation (12) (Gostiaux and van Haren, 2010; Mullison, 2017):

$$\mathrm{RL} = k_c(E - E_r) \tag{11}$$

$$RL = 10\log_{10}\left(10^{kc(E-Er)/10} - 1\right) \tag{12}$$

where E_r is the unknown reverberation as produced by instrumental and environmental noises that are uncorrelated with suspended-sediment particles, and Equation (12) is valid for signal-to-noise ratio in dB larger than 10 whereas Equation (11) applies for a lower ratio (Gostiaux and van Haren, 2010; Mullison, 2017). A reasonable assumption is to consider the unknown reverberation E_r with a negligible variation and not prevailing over the sediment backscatter. Under this assumption, the measured variability of the intensity level remains correlated with the corrected backscatter strength, $S_v - S_c$, and a decent calibration may be achieved between the corrected backscatter as assessed from field samples and the measured intensity level.

The k_c coefficient is a known conversion factor between counts and dB, which is available on request from the manufacturer or can be easily assessed with the hydrophone test described in Teledyne RD Instruments (1999). For the present study, and for the used ADCPs, k_c presented values of 0.4126, 0.4027, 0.4, 0.4028 and 0.3909, 0.4094, 0.4061, 0.412 for beam 1 to 4 and 600 kHz and 1200 kHz, respectively.

Since the undesired portion of the received signal is unknown for many applications in a natural riverine environment, the entire signal should be modeled by considering all the possible sources of underwater sound reverberation. Therefore, a general expression in dB is reported in Equation (13), which combines the received signal at the transducer (i.e. Equation (12)) and the corrected backscatter (Equation (1)):

$$EL + S_v - S_c = 10\log_{10}\left(10^{kc(E-Er)/10} - 1\right) \tag{13}$$

This equation may be applied for the calibration of E_r to match the corrected backscattering strength on the basis of observed sediment content. In addition, as suggested by Gostiaux and van Haren (2010) and Mullison (2017), the right-hand term of Equation (13) collapses to $k_c(E - E_r)$ when the signal-to-noise ratio is higher than 10, that is for $k_c(E - E_{bn}) > 10$. This simplification yields a linear relationship between the corrected backscatter and the received echo intensity.

Whatever the approach used (Equation (13) or its linearization for signal-to-noise ratio higher than 10), an important assumption is that the masking level is independent of space and time, which seems reasonable for a spot survey within a limited reach of a river. The same assumption is required in case of repeated surveys with different hydrologic conditions and for long-term monitoring. Therefore, practical applications may require repeated calibrations even when using the same devices, which are characterized by unchanged instrumental parameters (i.e. k_c and EL in Equation (13)). Given that an ADCP user may be interested in characterizing the devices, the calibration of the unknown reverberation (i.e. E_r) is herein maintained apart from the assessment of instrumental parameters.

Implication of transmitted power and acoustic pulse length

Following Deines (1999) and Mullison (2017), among others, the emitted level, EL in dB, can be expressed by means of the transmitted power, P_T, the pulse length, L, and the parameter C, which defines the transducer's geometry and efficiency. Accounting for this detailed description of the ADCP features and the presented formulations for the corrected backscatter, the suspended-sediment concentration is herein expressed in dB (Equation (14)) by rearranging and substituting Equations (8), (9), (10) and (12) into Equation (13).

$$10\log_{10}(K_{s1}M_{s1} + K_{s2}M_{s2}) = 10\log_{10}\left(10^{kc(E-Er)/10} - 1\right) + 2(\alpha_w + \alpha_s)R + 10\log_{10}\left(\frac{T_t R^2 \psi^2}{LP_T}\right) + C \tag{14}$$

From Equation (14) it is emphasized that any variation in the transmitted power, which changes with the efficiency of the powering source of the used device, can significantly affect the acoustic balance. To determine the effect of varying power sources on transmitted power and Equation (14), ADCPs were powered by different sources including old (survey Aa) and new (survey Ab) batteries and an alternating current inverter (survey B).

The transmitted power should be computed for each study case by applying Equations (15) and (16) for 1200 and 600 kHz frequencies, respectively, using the raw data from Teledyne RD Instruments ADCPs, that include the actual values of the transmitted current, TC, and transmitted voltage, TV (Scott Idle, Teledyne RD Instruments, personal communication).

$$P_{T1200} = (0.011451\mathrm{TC}) \times (0.253765\mathrm{TV}) \tag{15}$$

$$P_{T600} = (0.011451\mathrm{TC}) \times (0.380667\mathrm{TV}) \tag{16}$$

The length of the emitted acoustic pulse, L, is also recorded in the ADCP binary file. According to the frequency and the cell size used, for the present work, L was equal to 0.35 m and 0.71 m for 1200 kHz and 600 kHz, respectively.

The additional instrumental constant, C, is typically equal to −129.1 dB and −139.3 dB for 1200 kHz and 600 kHz, respectively. The same constant can be assessed under Deines (1999) and Mullison (2017).

Calibration procedure and considerations

The unknown reverberation, which is not related to suspended-sediment particles, E_r, was assessed with Equation (14) by entering the instrument parameter values, the echo intensity level from ADCPs and the corrected backscatter at each sampled point. PSD and sediment concentration values of wash load and suspended-sand fractions at each zone and sampled point also were entered. Note that in cases of prevailing backscatter from sand (i.e. $K_{s2} >> K_{s1}$), Equation (14) further simplifies to Equation (17), which also assumes $k_c(E - E_{bn}) > 10$.

$$\log_{10}[K_{s2} \cdot M_{s2}(R)] = 0.1\,[S_T(R)] + K_T \tag{17}$$

where K_T includes the parameters C, P_T, L, and E_r presented in Equation (14) and S_T is the corrected signal (Equation (18)),

$$S_T = k_c E + 2(\alpha_w + \alpha_s)R + 10\log_{10}\left(T_t R^2 \psi^2\right) \tag{18}$$

When the range-dependent suspended-sediment concentration of the sand fraction, M_{s2}, is producing the major backscatter strength, the slope coefficient of the linear regression in Equation (17) should be equal to 0.1. This simple equation can be used in the first instance to elucidate the fraction of particle size that produces the higher backscatter strength when complex bi- or multi-modal PSD, variation of particle size along the water column occur or different wash load/sand concentration ratios are present. In that way, the acoustic response could be evaluated to eventually apply Equation (14).

Note that when the sound absorption due to sand particles is substantial, both sides of Equation (14) depend on sand content, which implies an iterative method to assess the actual concentration of sand, M_{s2} (Thorne and Hanes, 2002).

The acoustic frequency greatly influences the measured echo intensities. The frequency-dependent sensitivities of backscatter and sound attenuation due to suspended-sediment particles play a relevant role in Equation (14) and in the rest of the derived forms. In fact, the form factor, f, and the sound absorption coefficient due to suspended sediment, α_S, depend on the wavenumber-particle radius product x and, therefore, acoustic frequency.

Results

Suspended-sediment characteristics from samples

Values of d_{50} (i.e. the size for which 50% of the material is finer in the number distribution) and corresponding geometric deviation of suspended sand and wash load fractions are presented in Table I for Zones A and B at each of the measured verticals. The wash-load concentration, M_{s1}, is composed of 32% clay and 68% silt at Zone A and 30% clay and 70% silt at Zone B. The PSDs of these fine fractions are homogeneous across the channel and among the verticals and are classified as very poorly sorted ($2 < \sigma < 4$) by Blott and Pye (2001).

In Zone A, measured suspended sand was very fine and fine sand. The percentage of fine sand at 0.2 h is approximately 50% of the total sand volume sampled and increases to 60% in samples collected close to the riverbed. The corresponding mean diameter shows small variations both across the river channel and along the water depth in Zone A (see Table I). As expected, the PSD of sand is narrower than the one observed for wash load. Sand is moderately/poorly sorted ($1.0 < \sigma < 1.6$) for samples from Zone A. Note that both fractions' PSDs follow normal distributions.

The profiles of suspended-sediment concentration at investigated verticals and for both macro classes (i.e. M_{s2} and M_{s1} contents of particles larger and smaller than 62 μm, respectively) reflect a noticeable vertical gradient for sand concentration (Figure 2). On the contrary, wash-load concentration was observed with an almost homogenous concentration along the water column (Figure 2), although the concentration of this class noticeably changed among different dates in Zone A (mean values of 420 mg l^{-1} and 74 mg l^{-1} for surveys Aa and Ab, respectively) and for different locations across the river channel in Zone B (mean values of 61 mg l^{-1}, 1381 mg l^{-1} and 7 mg l^{-1} at verticals B1, B2–B3 and B4, respectively).

The suspended-sand concentration, M_{s2}, changed from −100% to 150% of the corresponding depth-integrated value when moving from sampling levels close to the water surface to the riverbed, respectively. Minor deviations were observed at the B4 vertical, where the lowest depth-averaged M_{s2} (< 10 mg l^{-1}) was sampled. The wash-load fraction appeared homogeneously distributed in the water columns at Zones A and B (verticals B2 and B3). In this case, the deviations along the vertical were limited to ±6% of the depth-integrated value, except for vertical B1 where wash-load concentration increased significantly close to the bottom. This may indicate a density current produced by heavily laden inflow of the Paraguay River into the almost clear water of the upper Paraná River. Wash-load concentration, M_{s1}, was very low in vertical B4, and the corresponding distribution along the water depth was insignificant in respect to the sampling and laboratory analysis accuracy.

Corrected backscatter and suspended-sediment concentration

A simplified approach was considered when analyzing the influence of PSD on calibrations between corrected backscatter and suspended-sediment concentration. The full suspended-sediment PSD from samples was reduced to two macro classes

Table I. Number distribution particle sizes in micrometers corresponding to the content of the two macro classes considered: clay–silt (M_{s1}) and sand (M_{s2}) near surface (0.2 h) and bottom (0.9 h)

Zone A	Sample (μm)	Aa1 (0.2 h)	Aa1 (0.9 h)	Aa2 (0.2 h)	Aa2 (0.9 h)	Aa3 (0.2 h)	Aa3 (0.9 h)	Aa4 (0.2 h)	Aa4 (0.9 h)	Aa5 (0.2 h)	Aa5 (0.9 h)
	d50	7	7	7	7	6	7	7	7	7	8
Ms1	σ	2.9	2.9	2.9	2.9	2.6	2.8	2.8	2.8	2.8	2.9
	d50	85	86	87	93	80	83	85	86	87	83
Ms2	σ	1.3	1.4	1.3	1.3	1.5	1.3	1.4	1.4	1.4	1.4

Zone B	Sample (μm)	B1 (0.9 h)	B2 (0.2 h)	B2 (0.9 h)	B3 (0.2 h)	B3 (0.9 h)	M_{s1}^a
M_{s2}	d_{50}	106	104	105	104	109	4
	σ	1.9	1.9	1.9	1.9	1.9	3

[a]Mean of depth averaged values from verticals B2 and B3.

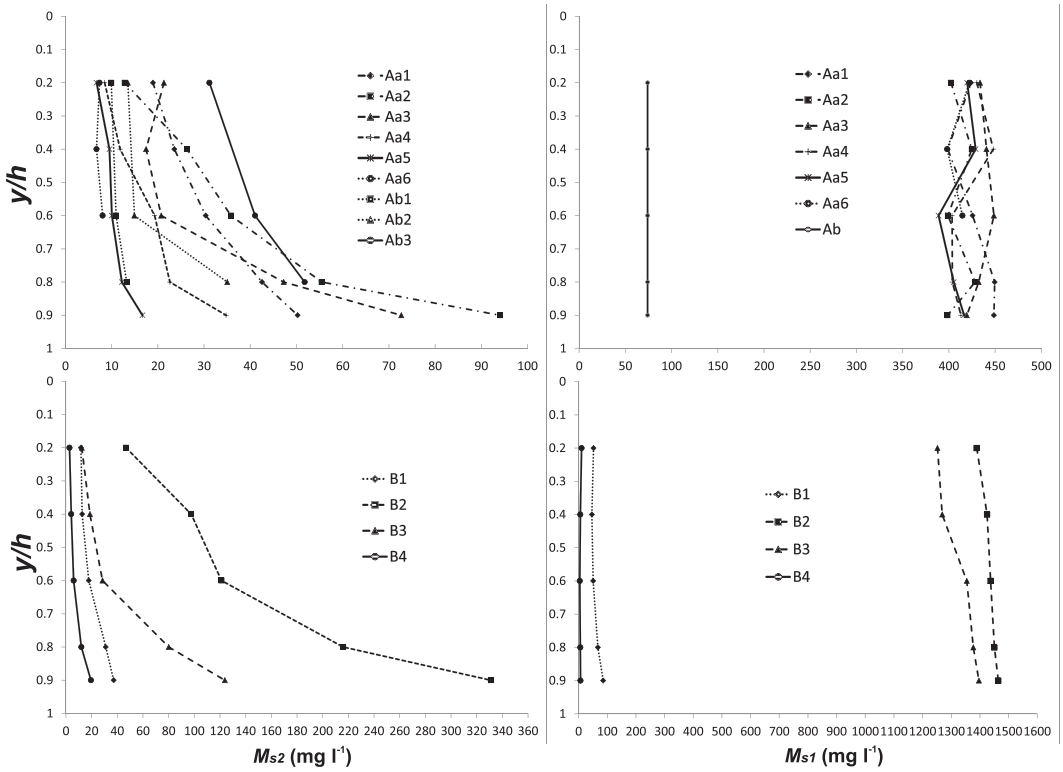

Figure 2. Concentration profiles of suspended sand (M_{s2}) and clay–silt (M_{s1}) for the measured verticals at the two investigated zones.

separated by 62 μm size, which represented the suspended sand from the riverbed and clay–silt forming the wash load from the upstream basin. The attenuation coefficients and backscatter were modeled based on median values for the d_{50} corresponding to sand and wash-load fractions, as measured at survey Aa and Zone B (Table I). Note that the particle sizes at Zone A (surveyed on March 17, 2014, survey Aa) were assumed constant with the same values for survey Ab (surveyed on September 20, 2014) because particle size analyses were not performed for the latter measurement.

The calibrations between sand concentration (M_{s2}) and the corresponding corrected signal (Equation (17)) for both ADCP frequencies in the studied sites are presented in Figure 3. For surveys Aa and Ab (Figure 3a), similar linear fits were obtained for both frequencies. The R^2 values were equal to 0.87 and 0.93 for 600 and 1200 kHz in survey Aa, respectively, and 0.94 in the Ab survey (1200 kHz), with corresponding slope coefficients of 0.1 and 0.11 in survey Aa (600 and 1200 kHz, respectively) and 0.09 in survey Ab. These slope coefficients are very close to the theoretical value of 0.1 as reported in Equation (17), which indicates the sand fraction dominates the backscatter measurement. As will be explained in more detail in the next sections, backscatter from the wash-load fraction is negligible compared to backscatter from the sand fraction; therefore, no direct correlation was found between wash-load sediment and corrected backscatter. However, wash-load concentration values from samples were used to correct the corresponding acoustic signal, by assessing the contribution of this macro class to the acoustic sediment attenuation coefficient, α_S, as described in Latosinski *et al.* (2014).

A similar result was observed for Zone B, where the slope coefficient was equal to 1.1 and R^2 0.92. High deviations from the calibrations were found for the first three points in vertical B1 (i.e. for 0.2, 0.4, 0.6 *h*). These deviations reflect the poor mixing of heavily laden flow from the Paraguay River into the main channel of the Paraná River, which commonly results in increasing gradients of the mixture density towards the riverbed (Lane *et al.*, 2008; Ramón *et al.*, 2014; Trevethan *et al.*, 2015). In addition, deviations from the calibrations were found for point sample locations with low concentrations of

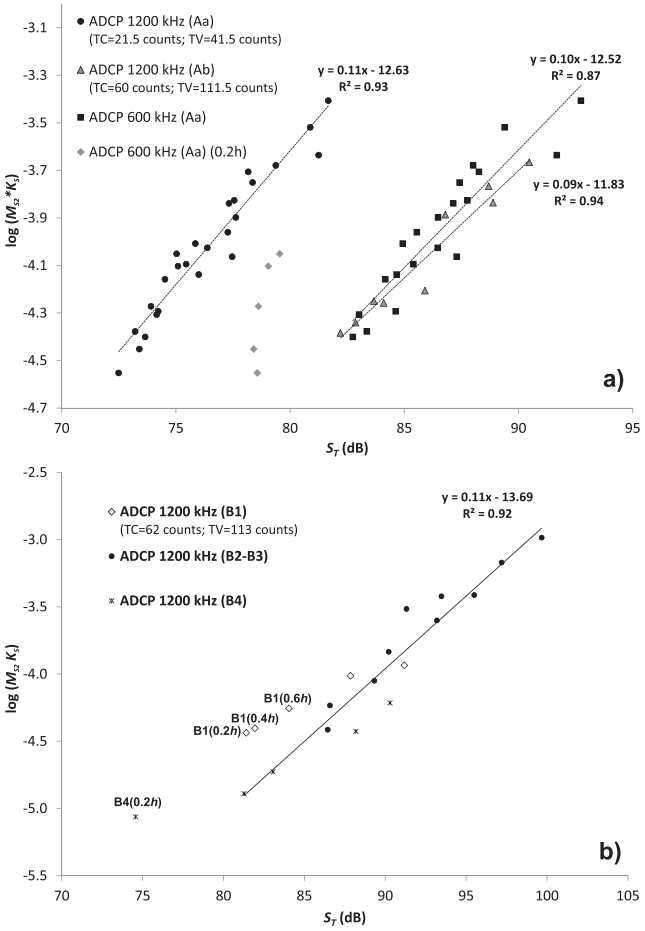

Figure 3. Relation between corrected signal S_T and suspended-sand concentration M_{s2} at Zones A (a) and B (b).

suspended sand (as in some points of verticals B1 and B4 in Figure 3b). These deviations reflect a lower echo intensity level response due to lower sand concentrations and the influence of other possible processes of scattering (e.g. flocs and organic matter scattering). It is worth mentioning that for a low concentration of sand, the corresponding echo intensity level, E, is likely to approach the noise level E_r; therefore, the assumed simplification presented by Deines (1999) may not be applied.

Different behaviors among the frequencies used are observed in the area near the ADCP transducers (points measured at 0.2 h). Note that the near-surface values (i.e. 0.2 h) from 600 kHz ADCP noticeably deviate from the fitted regression (Figure 3a), while this behavior is not observed for 1200 kHz ADCP. For each vertical measured in survey Aa, the first sampled points are located between 1 m and 1.43 m from the water surface, close to the critical limit distance at which the beam can be considered to have fully formed (Mullison, 2017). According to Deines (1999) the use of the backscatter equation should be limited to beyond $(\pi/4) \times$ Rayleigh distance for the given instrument, which is equal to 1.37 m and 1.34 m for 600 kHz and 1200 kHz Rio Grande ADCPs, respectively. Henceforth, near-surface values (0.2 h) for the 600 kHz ADCP were not considered in the following analysis.

It is important to highlight the same slope coefficients but different intercept values of the corresponding calibration (K_T in Equation (17)) for the different survey and same ADCP frequency (see 1200 kHz ADCP dataset for surveys Aa and Ab in Figure 3a). This behavior can be explained by the different power sources used at each survey zone. As previously mentioned, the same battery was used for both ADCPs in survey Aa. In this case, the transmitted current (TC) and transmitted voltage (TV) were 21.5 counts and 41.5 counts, respectively. A new battery was used in survey Ab, resulting in TC and TV values equal to 60 and 111.5 counts, respectively. In Zone B, alternating current was used, and TC and TV values were 62 and 113.5 counts, respectively. No significant changes (±1 count) were observed for TC and TV during the approximately eight hours at each survey.

As expected, data obtained using the same power source but different frequency ADCPs resulted in different relationships, which reflect not only the variation in acoustic frequency response to suspended sediment but also the effect of different instrument parameters (C and L), noise level (E_r) and sediment and fluid attenuation correction, as presented in the following sections.

Noise level calibration

The noise level both from equipment and environment, E_r, was calibrated by applying sediment concentration and particle size from samples at each point and corresponding ADCP at survey Aa, eventually assessing E_r with Equation (14). In the following sections, this full acoustic equation and noise level obtained in survey Aa is evaluated at survey Ab and Zone B. Note that E_r was evaluated using approaches in Deines (1999) (Equation (11)) and Mullison (2017) (Equation (12)) to eventually elucidate the deviation between these two approaches for the different signal-to-noise ratio presented at each zone. In addition, the full number PSD was considered to assess the acoustic parameters in Equations (9) and (10). This elucidates the deviation in the resulting E_r when considering only the median diameters (d_{50}) of each macro classes and full PSD.

In Table II, mean noise values ($\overline{E_r}$) are presented for each acoustic frequency using dataset obtained at survey Aa. It is worth noting that E_r did not appear to be range- and time-dependent, presenting random deviation values for the different locations and depths across the channel section. These $\overline{E_r}$ values averaged 16.8 and 19.5 dB for 1200 kHz and 600 kHz frequencies, respectively, considering a median particle size. Computations of $\overline{E_r}$ considering the PSD at each point deviate −0.6% and −5% from the computations using d_{50} values for the 1200 kHz and 600 kHz ADCPs, respectively. Note that less than 0.1% deviations were observed among calibrated values of E_r under Deines and Mullison formulations, i.e. the term $k_c(E - E_r)$ is larger than 10 for either used frequency and for all measured points.

Table II. Values of noise level (E_r) obtained for each frequency at survey Aa

	1200 kHz		600 kHz	
	E_{rPSD}[a]	E_{rd50}[b]	E_{rPSD}[a]	E_{rd50}[b]
$\overline{E_r}$	16.7	16.8	20.6	19.5
Standard deviation	1.2	1.1	1.27	1.18
Maximum	19.4	19.2	22.3	22.4
Mininum	14.4	14.9	17.6	17.5
RD (%)[c]	—	-0.6	—	−5

[a]Considering full particle size distribution (PSD) in Equations (9) and (10).
[b]Considering d_{50} value (i.e. the size for which 50% of the material is finer in the number distribution) for each macro class.
[c]Relative difference (RD) = $[(E_{rd50} - E_{rPSD})/E_{rPSD}] \times 100$.

On average, the difference in E_r considering PSD at each point sampled is 0.1 dB and 1.1 dB for the frequencies of 1200 kHz and 600 kHz, respectively. These differences are produced by changes in sediment attenuation coefficient $\langle \alpha_s \rangle$ and the backscatter coefficients $\langle K_{si} \rangle$ when full PSD is considered (see Equations (9) and (10)). On average, $\langle \alpha_s \rangle$ increases 25% and 55% for 1200 kHz and 600 kHz, respectively, when full PSD is considered compared with median particle size. For $\langle K_{si} \rangle$, the increment is 94% and 7% in the case of wash-load and sand fractions, respectively, for both frequencies. However, the impact of these changes in $\overline{E_r}$ is negligible for the 1200 kHz ADCP, on the order of the standard deviation value for 600 kHz (see Table II). In the following section, the role that these terms and its variation play in Equation (14) is discussed.

Validation between measured and estimated sand concentration for all survey zones

Sampled and acoustically inferred concentrations of suspended sand (M_{s2}) are compared for each survey zone in Figure 4, using each ADCP frequency and the mean values as reported in Table II, i.e. $\overline{E_{r\,d50}}$ and $\overline{E_{r\,PSD}}$. Using $\overline{E_r}$ values as calibrated in Zone A, the acoustic assessment of M_{s2} was validated in verticals Aa6, Aa7 and survey Ab (Figures 4a and 4b, points in color) and Zone B (Figure 4c). For Ab zone, a d_{50} value corresponding to that measured at survey Aa was used.

Two major aspects may be argued. The first aspect refers to the dispersion of the data when an average value of E_r is assumed. Table III shows the average deviations of M_{s2} with the corresponding maximum and minimum values computed. In survey Aa, average and maximum deviations are less than 2% and ±50%, respectively, for the 1200 kHz ADCP; these values roughly double for the 600 kHz ADCP. Secondly, a reasonable validation (maximum average deviation of 41%, see Table III) is obtained for verticals Aa6 and Aa7, survey Ab and Zone B by applying the calibration developed at survey Aa. However, concentrations were overestimated at all points for survey Ab (mean value of 30% with a maximum of 76% difference from

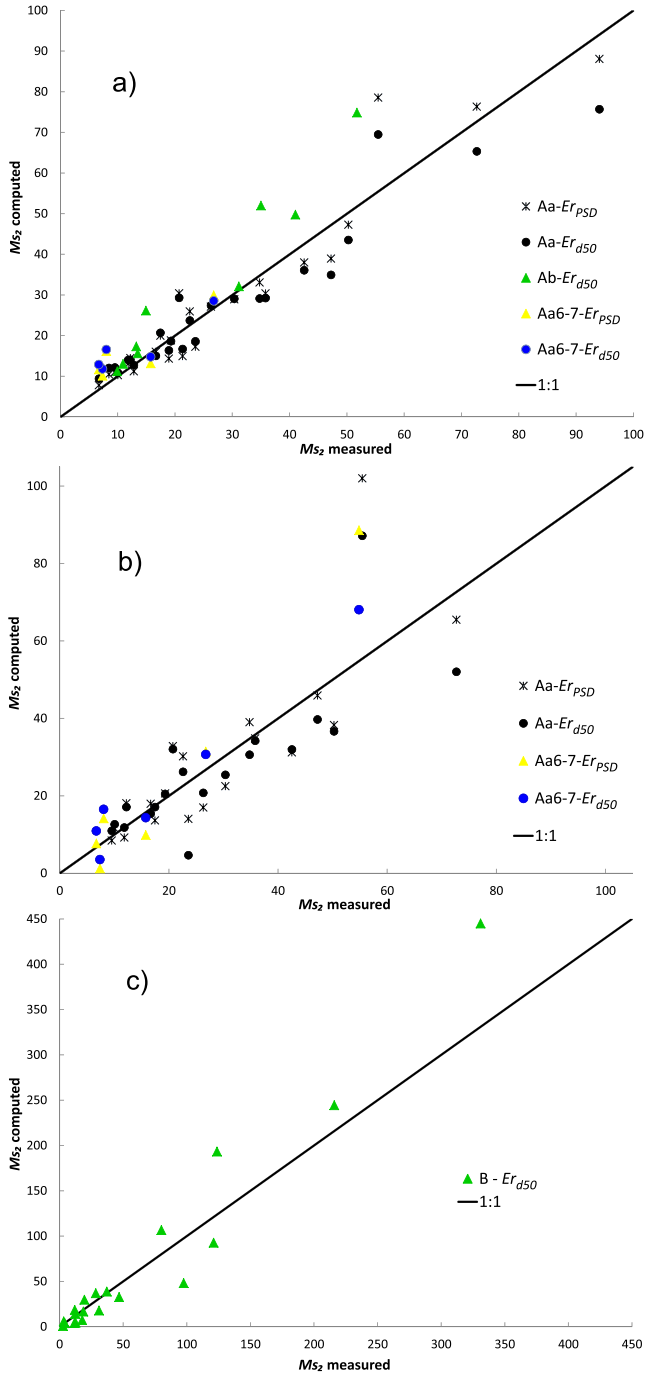

Figure 4. Comparison of M_{s2} measured versus computed using Equation (14): (a) 1200 kHz acoustic Doppler current profile (ADCP), surveys Aa and Ab; (b) 600 kHz, survey Aa; (c) 1200 kHz ADCP, Zone B. Note that in Table II $\overline{E_r}$ was obtained only in survey Aa and was used for verticals Aa6, Aa7, survey Ab and Zone B. [Colour figure can be viewed at wileyonlinelibrary.com]

measured, see Figure 4a). Note that in survey Ab, the assumed d_{50} was actually measured in survey Aa. In fact, given the higher water stage at survey Ab, larger diameters of particles in suspension would be expected, indicating the importance of having the actual size of suspended sand for an accurate inversion of Equation (14).

Impact of sand and wash-load sediment fractions on sound attenuation

Attenuation coefficients varied over the conditions analyzed (Figure 5), depending on the zone and verticals characterized by different particle sizes, sand and wash-load concentrations, temperature and frequencies employed. In Figure 5, α_S was computed using a d_{50} value of each macro class. Note that this coefficient increases when full PSD is considered according to the analysis previously presented in this article. The variation in the attenuation coefficient related to the wash-load fraction (α_{s1}), mimicked concentration changes among the investigated zones and verticals. Maximum attenuation values (80–90% of the total attenuation) in B2 and B3 verticals corresponded to mean M_{s1} of 1381 mg l^{-1}, whereas the attenuation decreased to 23% and 5% of the total at B1 and B4 verticals where wash-load concentrations were 61 and 7 mg l^{-1}, respectively. At survey Aa, the attenuation from wash-load sediments represented 53% of the total attenuation that was due to a homogeneous wash-load concentration of about 420 mg l^{-1}. This attenuation decreased to 10–20% of the total for survey Ab because of the lower observed wash load (M_{s1} equal to 74 mg l^{-1} on average). Due to homogeneous distribution M_{s1} in the water column at all study verticals, no substantial changes in attenuation were observed in the water column, between 0.2 and 0.9 h.

For all the analyzed cases, the sand fraction α_{s2} showed a negligible attenuation, with values lower than 1%, although M_{s2} varied from approximately 0 (vertical B4) to 340 mg l^{-1} (verticals B2–B3). Due to the increase in suspended sand with depth, the $\alpha_{s2(0.9h)}/\alpha_{s2(0.2h)}$ ratio was equal to two for all verticals, except verticals B3 and B4 (verticals with the highest sediment concentration gradient) where these ratios increase to three and four, respectively.

For the 600 kHz ADCP (survey Aa), α_{s1} was a larger portion of the total attenuation than for the 1200 kHz ADCP, which mostly reflected a decrease in water attenuation α_W rather than an increase of α_{s1}. In fact, α_W was about 0.25 dB m^{-1} on average for the 1200 kHz ADCP and decreased to 0.062 dB m^{-1} for the 600 kHz (survey Aa) while α_{s1} changed from 0.3 to 0.2 dB m^{-1} for each frequency, respectively.

Different attenuation terms affected the corrected backscattering strength, S_T in Equations (14) and (17). Each term contributing to the corrected backscattering strength is reported in Figure 6 for the analyzed zones, in percent of the total S_T.

The attenuation produced by sand fraction ($2\alpha_{s2}R$) was 0.03% and 0.05% of S_T on average along the water column for 1200 and 600 kHz, respectively. The attenuation produced by the wash-load fraction ($2\alpha_{s1}R$) for 1200 kHz was 3%, 0.6%, 8% and 0.3% of S_T in surveys Aa, Ab, B2–B3 and

Table III. Relative suspended-sediment concentration (M_{s2}) difference (%) for each case, acoustic Doppler current profiler (ADCP) frequency and study zone

	Aa 1200 kHz		Aa 600 kHz		Aa6–Aa7 1200 kHz		Aa6–Aa7 600 kHz		Ab 1200 kHz	B 1200 kHz
	$\overline{E_{r\,PSD}}$	$\overline{E_{r\,d50}}$	$\overline{E_{r\,PSD}}$	$\overline{E_{r\,d50}}$	$\overline{E_{r\,PSD}}$	$\overline{E_{r\,d50}}$	$\overline{E_{r\,PSD}}$	$\overline{E_{r\,d50}}$	$\overline{E_{r\,d50}}$	$\overline{E_{r\,d50}}$
Average	1.8	1.8	4.7	3.8	41	41	8	24	30.8	−3.1
Maximum	46.7	42.6	83.9	57.2	106	106	76	105	76.2	73.3
Minimum	−29.9	−28.0	−40.5	−28.4	−10	−9	−84	−53	3.6	−70.8

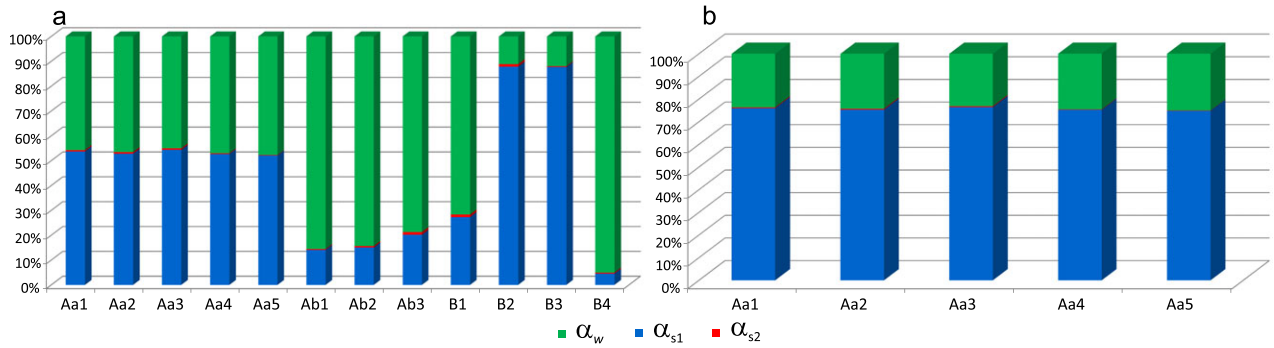

Figure 5. Percentage of depth averaged attenuation due to clear water, α_W, clay–silt and sand macro classes, i.e. α_{s1} and α_{s2} corresponding to M_{s1} and M_{s2} concentration, respectively. Different zones (A and B) and hydrological conditions (Aa and Ab) were analyzed by means of the 1200 kHz (a) and 600 kHz (b) acoustic Doppler current profilers (ADCPs). [Colour figure can be viewed at wileyonlinelibrary.com]

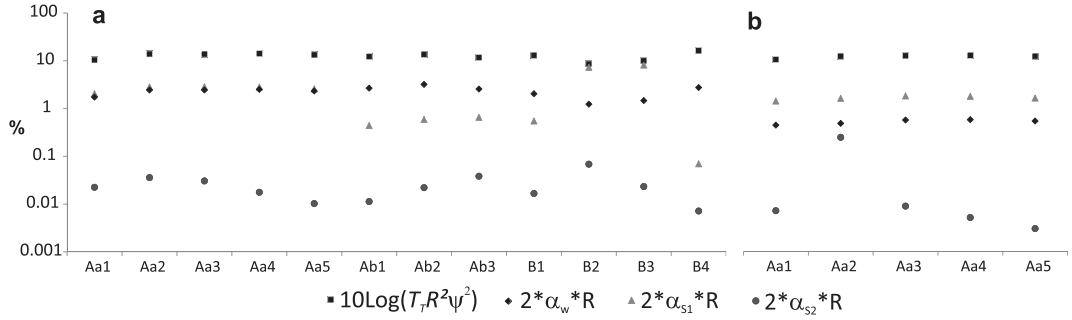

Figure 6. Percentages of depth averaged values of the terms forming the corrected backscatter S_T (see Equation (19)) for different zones and 1200 kHz (a) and 600 kHz (b) acoustic Doppler current profilers (ADCPs).

B1–B4, respectively, reflecting the corresponding concentration changes among zones. The wash-load fraction represented 1.7% of S_T for the 600 kHz ADCP in survey Aa, on average. Note that the major contribution to the corrected backscattering strength corresponded to beam spreading, which was about 12% for both frequencies.

Disregarding corrections produced by attenuation from the wash-load ($2\alpha_{s1}R$) and sand ($2\alpha_{s2}R$) fractions resulted in underestimations of M_{s2} equal to 12% and 0.5%, respectively, in survey Ab, underestimations of M_{s2} equal to 37% and 0.3%, respectively, in survey Aa, which were reduced to 27% and 0.9% when using the 600 kHz ADCP. The underestimations of M_{s2} for Zone B were −80% in verticals B2–B3, −6% in vertical B1 and −0.3% in vertical B4, when the wash-load fraction attenuation was disregarded. These underestimations in Zone B were reduced to less than 1% by disregarding sand fraction attenuation.

Backscattering strengths analysis

Following Hanes (2012) and Agrawal and Hanes (2015), the ratio between the sand and wash-load fractions' backscattering strength (Equation (19)) was evaluated:

$$\frac{\sigma_{s2}}{\sigma_{s1}} = \frac{f_2^2[M_s/(\rho_s a)]_2}{f_1^2[M_s/(\rho_s a)]_1} \tag{19}$$

These assessments considered d_{50} particle size presented in Table I for each zone. For all the study zones and verticals, the sand backscattering strength (σ_{s2}) was much higher than corresponding values of the wash-load fraction (σ_{s1})σ_{s1} (Figure 7). The backscattering ratio changed between surveys, from 9 to 15 in survey Aa and from 24 to 36 in survey Ab as

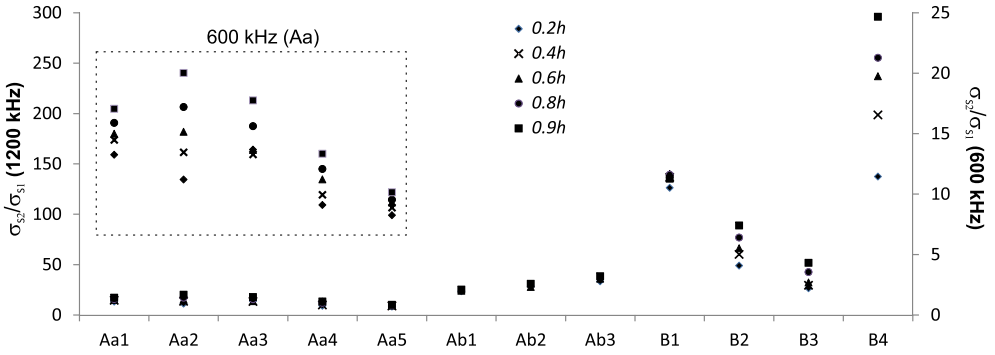

Figure 7. Backscattering strengths ratio of sand over clay–silt fractions for each vertical and zone investigated. [Colour figure can be viewed at wileyonlinelibrary.com]

averaged along verticals, the latter values reflecting lower concentrations of wash-load fraction.

The same behavior was observed with both ADCP frequencies; however, the scattering intensity produced by the 1200 kHz ADCP is four times higher than 600 kHz as a consequence of the higher value wavenumber introduced in the form factor.

In Zone B, the backscattering ratio was higher than in surveys Aa and Ab because of higher concentrations of sand. In verticals B2 and B3, the ratio increased with depth because of higher observed sand concentration gradients along the vertical (similar to the 600 kHz behavior in survey Aa). In vertical B4, small wash-load concentration yielded high backscattering ratios although lower backscattering strength from sand.

Despite the changes in the backscattering ratio presented in Figure 7, a good correlation is found between the sand-related corrected backscatter and sand concentration (Equation (17), Figures 3 and 4), which bore out a negligible effect of wash-load backscattering strength on measured echoes.

Discussion

According to the characteristics of the suspended sediment presented in the Paraná River system and used ADCP frequencies, the echo intensity level is governed by the sand fraction, and the wash-load fraction contributes negligible echo intensity level for all the wide ranges of concentrations measured at different zones and water stages in this study. These observations can be explained by the behavior of the form factor (f) in relation to sediment particle size and both ADCP frequencies (see Thorne and Hanes, 2002). The proposed acoustic method for estimating suspended-sand concentration resulted in mean deviations within about 40% from sampled concentrations for all survey locations and less than 10% for survey locations Aa with both ADCPs, survey Aa6–Aa7 with the 600 kHz ADCP, and Zone B with the 1200 kHz ADCP.

The obtained E_r values suggest that for typical PSD and concentration presented in sand bed rivers like the Paraná and Colastiné Rivers, the term $k_c(E - E_r)$ is broadly greater than 10 and therefore, the different formulations presented by Deines (1999), Gostiaux and van Haren (2010) and Mullison (2017) provided similar results. However, caution should be taken in deep streams with low sediment concentration that may result in low propagation of the acoustic signal with depth and low backscattering returns.

In addition, the simplification of the full PSD into the corresponding mean diameter of both fractions leads to deviations in the calibrated E_r. However, the observed deviations were lower than 0.1 and 1.1 dB for the 1200 kHz and 600 kHz ADCPs, respectively.

The assessed values of E_r were expected to account for the instrument noise (E_{ri}), the environmental noise (E_{re}), and the uncertainty in each term presented in Equation (14). Therefore, E_{re} could be produced by any interference such as a radio modem, echo sounder, ship noise or another acoustic instrument operating at a similar frequency as the used ADCPs. To assess instrument and environmental noise, noise evaluations are recommended for each study site and measurement condition to eliminate interference that could affect the E_r value.

The value E_{ri} is the measured echo intensity level measured by the ADCP in the absence of any transmitted signal. It may be obtained from an intensity level at the end of each ensemble or, for the ADCPs used in this study, issuing a special command (PT3) to the ADCP when it is under water. Note that for the used ADCPs, the E_{ri} value reported using these techniques was 46 counts (19 dB) for both frequencies, which were 2.2 dB higher and 0.5 dB lower than the computed E_r value obtained using Equation (14) (Table II) for 1200 kHz and 600 kHz, respectively. Note that these values are smaller than uncertainty (3 dB) of C parameter presented in Equation (14) (Deines, 1999). Additional studies are required to explain this difference, including an accuracy evaluation of each term in Equation (14) and other possible sources of uncertainty (e.g. the role of organic particles in backscatter, flocs, or other suspended particles or accuracy of the particle size information using the described analytical methods).

In general, the attenuation produced by the wash-load fraction had a role in the estimation of sand concentration for the investigated range of hydro-sedimentological conditions. Disregarding the attenuation produced by the wash-load fraction would have resulted in underestimation of the sand concentration by as much as 80% in the evaluated conditions, depending on the wash-load concentrations. On the contrary, the attenuation of the acoustic signal due to sand appeared negligible; ignoring the sand attenuation would have resulted in an underestimation of the sand concentration by less than 1% in the evaluated conditions.

The change in power supplied to the ADCPs was found to substantially change the TC and TV (see Figure 3 and different values of TC and TV in surveys Aa and Ab–B). Note that if TC and TV values using a new battery or generator with a power inverter (such as were used in survey Ab and Zone B) were used in Equation (14) at survey Aa (where battery power was poor), the value of E_r would have been underestimated by 68%, underestimating sand concentration by 87% (as a mean value) at this zone. Therefore, the actual TC and TV values should be known (reported in the raw ADCP data file) and should be used in calculations to account for TC and TV changes due to varying power.

Several factors may result in poor calibrations between suspended-sand concentration and the corrected backscattering strength (see dispersion presented in Figures 3 and 4) or may invalidate or cause deviations from an existing calibration. The first factor refers to how field measurements are made. Given the ADCP beams' divergence, difficulties in maintaining a stationary position for the boat, and any difference in sediment sampling location relative to the ADCP deployment location, an exact coincidence between the ADCP-measured and physically sampled water volume is rarely achieved. The second factor refers to simplifications in modeling sound propagation through water. Processes in addition to the backscatter response from the sand fraction and attenuation from the wash-load fraction may have an effect on the acoustic signal, such as water density and sediment stratification due to confluence mixing, temperature stratification, sediment flocculation, and presence of particle organic matter. However, reasonable calibrations (Figure 3) and constant values of E_r (Table II) were still found by simplifying some elements of the computations, particularly by reducing the full sediment PSD to two macro classes separated by the 62-μm size.

The simplifications required a site-dependent calibration to determine the noise level, E_r, assessed by fitting the corrected backscatter to sampled concentration of suspended sand. For the case of the Paraná River system, this calibration gave a constant E_r value close to the instrument noise irrespective of river zone and hydrologic condition, which corroborates the reliability of the operated simplifications. However, future validation at different rivers with varying sediment conditions is recommended, especially where grain size varies spatially (across the cross-section and with depth) and with hydrological condition.

Although ranges in observed particle sizes were fairly wide (Table I), similar regression lines and constant E_r value were

obtained using a mean particle size for each fraction when acoustically inferred and sampled sand concentrations were related through Equations (17) and (14), respectively, therefore, the sound propagation was reasonably modeled by the variation of backscattering strength and viscous attenuation related to sand and wash-load concentration changes, respectively.

Note that these results provide an important simplification when applying this methodology to other rivers as although median particle size across the section is necessary to know, it does not require the precise knowledge of the full PSD of the suspended material. However, more research is needed at sand bed river sites with even greater variation of PSD with depth in the water column than was measured in this study.

To finish, this article demonstrates that an acoustic methodology, using commercially-available ADCPs, enables the simultaneous investigation of flow velocity and sand concentration with a spatial (nearly complete cross-section) and temporal resolution impossible to achieve with traditional methods. These results are relevant for various research disciplines and water resources management agencies trying to weigh sediment sampling efforts and associated costs in medium and large rivers. In particular, the methods described in this article would be useful for rapidly quantifying suspended-sand distribution along a river channel to understand the dynamic interaction of flow and sediment transport. This knowledge could then support prediction of river channel morphodynamics (see for example Szupiany *et al*. [2012] and Hackney *et al*. [2018]), sedimentation and scour patterns near in-channel structures, reservoir infilling and sustainability, suitability of aquatic habitat, and transport of sediment-associated pollutants.

Note that many sand bed rivers throughout the world have similar sediment characteristics as those presented in the studied river (Paraná) (i.e. bi-modal suspended sediment [fine fraction transported as wash load and coarse fraction from the bed], see Latrubesse *et al*., 2005; Fielding, 2007; Latrubesse, 2015). The proposed acoustic calibration methodology provides a complete procedure to be applied in other rivers that have substantial variations in suspended sand throughout the cross-section and with depth. In contrast with the sand fraction, the wash-load fraction is typically homogeneously distributed across the section and relatively easy to sample to obtain an estimate of total suspended-sediment concentration when combined with the acoustic calibration methodology for estimating suspended sand.

Conclusions

This study demonstrates that commercially available, down-looking ADCPs of commonly-used frequencies (1200 kHz and 600 kHz), can be used to infer information regarding suspended-sand concentrations in sand bed river systems. The use of commercially available ADCPs to estimate suspended-sand concentrations is particularly compelling compared to other indirect methods for measuring sediment because of the ability to leverage existing uses of the equipment for flow velocity and discharge measurements, and by extension, ability to compute sediment fluxes or loads. The calibration method described in this article can provide quantitative information about suspended sand with a resolution nearly impossible to achieve by traditional sampling methods alone. In this sense, the relevant theory and detailed field measurements described in this article were successfully integrated to provide a powerful demonstration of the ADCP's capability for measuring suspended sediment studies in many sand bed rivers throughout the world.

The behavior and impact of the different terms of the sonar equation under a typical bi-modal particle size distribution found in sand bed rivers were evaluated. The associated methodology requires knowledge of sediment characteristics such as d_{50} particle size of both wash load and sand macro classes of suspended sediment and clay–silt concentration to estimate total suspended-sediment concentrations. Although the described approach could be applied in a large range of rivers characterized by sand beds with varying concentrations of fine sediment forming the wash load, it requires a case-study validation of the simplifications of the acoustic equations, which in this case were achieved by means of the noise term, E_r, calibration.

Differences between measured and estimated sediment concentration using the described methodology for the datasets collected in the Parana and Colastine River system averaged around ±40% for all study zones. Given that the suspended-sediment characteristics of the rivers described in this study are similar to many other sand bed rivers, especially large river systems throughout the world (Latrubesse, 2015), the present analysis advances efforts to develop a general acoustic methodology that can provide more accurate and higher spatial and temporal resolution data for fluvial suspended-sediment studies. Though traditional sampling techniques would still be required to develop and periodically validate calibrations, the methodology could ideally be used to obtain an estimate of suspended-sediment concentration and load at any time, particularly when sampling is not safe or practical. Application of the methodology is therefore expected to result in a fundamental shift in sediment assessment studies, providing cost effective, accurate, and high-resolution sediment data that are essential for understanding the dynamics of sand bed river systems.

Acknowledgements—The authors would like to thank Mr Roberto Mir and Sr Santiago Cañete from Universidad Nacional del Litoral for their assistance during the fieldwork, MSc. Ana M. Alvarez and Dr Marcos Gallo for conducting suspended-sediment analysis, the National Institute of Limnology for providing the US P-61 sampler, and Dr Daniel Parsons from University of Hull for providing the 600 kHz ADCP. Comments by Tim Straub, Daniel Hanes and Daniel Parsons for their technical review of the manuscript are greatly appreciated. This study is part of the project 'Fluvial process studies in large rivers using acoustic Doppler technology' granted by the Universidad Nacional del Litoral, Argentina. Any use of trade, firm, or product names is for descriptive purposes only and does not imply endorsement by the US Government.

References

Agrawal YC, Hanes DM. 2015. The implications of laser-diffraction measurements of sediment size distributions in a river to the potential use of acoustic backscatter for sediment measurements. *Water Resources Research* **51**(11): 8854–8867. https://doi.org/10.1002/2015WR017268.

Blott SJ, Pye K. 2001. Gradistat: a grain size distribution and statistics package for the analysis of unconsolidated sediments. *Earth Surface Processes and Landforms* **26**: 1237–1248. https://doi.org/10.1002/esp.261.

Clay CS, Medwin H. 1977. *Acoustical Oceanography: Principles and Applications*. Wiley: Hoboken, NJ.

Davis BE. 2005. *A Guide to the Proper Selection and Use of Federally Approved Sediment and Water-quality Samplers*, US Geological Survey, Open File Report 2005-1087. US Geological Survey: Vicksburg, MS; 20 pp.

Deines KL. 1999. Backscatter estimation using broadband acoustic Doppler current profilers. In Proceedings, *Sixth Working Conf. on Current Measurement*, San Diego, CA. IEEE, 249–253.

Drago E, Amsler ML. 1988. Suspended sediment at a cross section of the middle Paraná River: concentration, granulometry and influence of main tributaries. In *Proceedings, Symposium on Sediment Budgets*,

International Association of Hydrological Sciences No. 74. IAHS Press: Wallingford; 381–396.

Drago E, Amsler ML. 1998. Bed sediment characteristics in the Paraná and Paraguay Rivers. *Water International* **23**: 174–183.

Downing A, Thorne PD, Vincent CE. 1995. Backscattering from a suspension in the near-field of a piston transducer. *Journal of the Acoustical Society of America* **97**(3): 1614–1620.

Edwards TK, Glysson DG. 1999. *Techniques of Water-resources Investigations of the U.S. Geological Survey. Applications of Hydraulics. Field Methods for Measurement of Fluvial Sediment*. US Geological Survey: Reston, VA; Book 3, Chapter C2, p. 89.

Fielding CR. 2007. Sedimentology and stratigraphy of large river deposits: recognition in the ancient record, and distinction from "incised valley fills". In *Large Rivers: Geomorphology and Management*, Gupta A (ed). John Wiley & Sons: Chichester; 97–113.

Gartner JW. 2004. Estimating suspended solids concentrations from backscatter intensity measured by acoustic Doppler current profiler in San Francisco Bay, California. *Marine Geology* **211**: 169–187.

Gray J, Glysson D, Edwards T. 2008. Suspended-sediment samplers and sampling methods. In *Sedimentation Engineering: Processes, Measurements, Modeling, and Practice*, Garcia M (ed), ASCE Manuals and Reports on Engineering Practice, N°110. American Society of Civil Engineers (ASCE): Reston, VA; 320–339.

Gray JR, Gartner JW. 2010. Surrogate technologies for monitoring bed-load transport in rivers. In *Sedimentology of Aqueous Systems*, Poleto C, Charlesworth S (eds). Wiley-Blackwell: London; Chapter 2; 46–79.

Gostiaux L, van Haren H. 2010. Extracting meaningful information from uncalibrated backscattered echo intensity data. *Journal of Atmospheric and Oceanic Technology* **27**(5): 943–949.

Guerrero M, Rüther N, Szupiany R, Haun S, Baranya S, Latosinski F. 2016. The acoustic properties of suspended sediment in large rivers: consequences on ADCP methods applicability. *Water* **8**(1): 13. https://doi.org/10.3390/w8010013.

Guerrero M, Szupiany RN, Latosinski F. 2013. Multi-frequency acoustics for suspended sediment studies: an application in the Paraná River. *Journal of Hydraulic Research* **51**(6): 696–707. https://doi.org/10.1080/00221686.2013.849296.

Hackney CR, Darby SE, Parsons DR, Leyland J, Aalto R, Nicholas AP, Best JL. 2018. The influence of flow discharge variations on the morphodynamics of a diffluence–confluence unit on a large river. *Earth Surface Processes and Landforms* **43**(2): 349–362. https://doi.org/10.1002/esp.4204.

Hanes DM. 2012. On the possibility of single-frequency acoustic measurement of sand and clay concentrations in uniform suspensions. *Continental Shelf Research* **46**: 64–66.

Hanes DM. 2016. Acoustic attenuation due to bi-modal size distributions of suspended sediment. *Journal of Coastal Research* **75**: 23–27.

Haught D, Venditti JG, Wright SA. 2017. Calculation of *in situ* acoustic sediment attenuation using off-the-shelf horizontal ADCPs in low concentration settings. *Water Resources Research* **53**: 5017–5037. https://doi.org/10.1002/2016WR019695.

Holdaway GP, Thorne PD, Flatt D, Jones SE, Prandle D. 1999. Comparison between ADCP and transmissometer measurements of suspended sediment concentration. *Continental Shelf Research* **19**: 421–441.

Kumar R, Strom K, Keyvani A. 2010. Floc properties and settling velocity of San Jacinto estuary mud under variable shear and salinity conditions. *Continental Shelf Research* **30**: 2067–2081.

Lane SN, Parsons DR, Best JL, Orfeo O, Kostaschuk RA, Hardy RJ. 2008. Causes of rapid mixing at a junction of two large rivers: Rio Parana and Rio Paraguay, Argentina. *Journal of Geophysical Research: Earth Surface* **113**(F2).

Landers MN, Straub TD, Wood MS, Domanski MM. 2016. Sediment acoustic index method for computing continuous suspended-sediment concentrations. In *US Geological Survey Techniques and Methods*. US Geological Survey: Reston, VA; Book 3, Chapter C5; 63.

Latosinski FG, Szupiany RN, García CM, Guerrero M, Amsler ML. 2014. Estimation of concentration and load of suspended bed sediment in a large river by means of acoustic Doppler technology. *Journal of Hydraulic Engineering* **140**(7): 1–15.

Latrubesse EM, Stevaux JC, Sinha R. 2005. Tropical rivers. *Geomorphology* **70**: 187–206.

Latrubesse EM. 2015. Large rivers, megafans and other Quaternary avulsive fluvial systems: a potential "who's who" in the geological record. *Earth-Science Reviews* **146**: 1–30.

Manaster AD, Domanski MM, Straub TD, Boldt, JA. 2016. *Estimating Suspended Sediment using Acoustics in a Fine-grained Riverine System on Kickapoo Creek at Bloomington, Illinois*, US Geological Survey Open-File Report 2016-1117. US Geological Survey: Reston, VA; 42 pp.

Moate BD, Thorne PD. 2013. Scattering from suspended sediments having different and mixed mineralogical compositions: comparision of laboratory measurements and theoretical predictions. *Journal of the Acoustical Society of America* **133**(3): 1320–1334.

Moore SA, LeCoz J, Hurther D, Paquier A. 2013. Using multi-frequency acoustic attenuation to monitor grain size and concentration of suspended sediment in rivers. *Journal of the Acoustical Society of America* **133**: 1959–1970.

Mueller DS, Wagner CR, Rehmel MS, Oberg KA, Rainville F. 2014. Measuring discharge with acoustic Doppler current profilers from a moving boat. In *US Geological Survey Techniques and Methods*, Vol. **3A-22**, Version 2.0. US Geological Survey: Reston, VA 95 pp.

Mullison J. 2017. Backscatter estimation using broadband acoustic Doppler current profilers – updated. *Proceedings, ASCE Hydraulic Measurements & Experimental Methods Conference*, Durham, NH, July 9–12.

Ramón CL, Armengol J, Dolz J, Prats J, Rueda FJ. 2014. Mixing dynamics at the confluence of two large rivers undergoing weak density variations. *Journal of Geophysical Research: Oceans* **119**: 2386–2402. https://doi.org/10.1002/2013JC009488.

Rasband W, Ferreira T. 2012. ImageJ. US National Institutes of Health: Bethesda, MD. http://rsb.info.nih.gov/ij/S

Reichel G, Nachtnebel HP. 1994. Suspended sediment monitoring in a fluvial environment. Advantages and limitations applying an acoustic Doppler current profiler. *Water Research* **28**(4): 751–761.

Sassi MG, Hoitink AJ, Vermeulen B. 2012. Impact of sound attenuation by suspended sediment on ADCP backscatter calibrations. *Water Resources Research* **48**: W09520. https://doi.org/10.1029/2012WR012008.

Schulkin M, Marsh HW. 1962. Sound absorption in sea water. *Journal of the Acoustical Society of America* **34**: 864–865.

Szupiany RN, Amsler ML, Parsons DR, Best JL. 2009. Morphology, flow structure and suspended bed sediment transport at two large braid-bar confluences. *Water Resources Research* **45**: W05415. https://doi.org/10.1029/2008WR007428.

Szupiany RN, Amsler ML, Hernandez J, Parsons DR, Best JL, Fornari E, Trento A. 2012. Flow fields, bed shear stresses, and suspended bed sediment dynamics in bifurcations of a large river. *Water Resources Research* **48**: W11515. https://doi.org/10.1029/2011WR011677.

Teledyne RD Instruments. 1999. *Using the 305A4205 Hydrophone to Identify the RSSI Scale Factors for Calibrating the Echo Strength Output of an ADCP*, Technical Note, FST-004. Teledyne RD Instruments: San Diego, CA. http://www.comm-tec.com/Library [30 October 2015].

Thevenot MM, Kraus NC. 1993. Comparison of acoustical and optical measurements of suspended material in the Chesapeake Estuary. *Journal of Marine Environmental Engineering* **1**: 65–79.

Thomas LP, Marino BM, Szupiany RN, Gallo MN. 2017. Characterization of the suspended particulate matter in a stratified estuarine environment employing complementary techniques. *Continental Shelf Research* **148**: 37–43. https://doi.org/10.1016/j.csr.2017.08.024.

Thorne PD, Hardcastle PJ, Soulsby RL. 1993. Analysis of acoustic measurements of suspended sediments. *Journal of Geophysical Research* **98**(C1): 899–910.

Thorne PD, Hardcastle PJ, Dolby JW. 1998. Investigation into the application of cross-correlation analysis on acoustic backscattered signals from suspended sediment to measure nearbed current profile. *Continental Shelf Research* **18**(6): 695–714.

Thorne PD, Hanes DM. 2002. A review of acoustic measurements of small-scale sediment processes. *Continental Shelf Research* **22**: 603–632.

Thorne PD, Meral R. 2008. Formulations for the scattering properties of suspended sandy sediments for use in the application of acoustics to sediment transport processes. *Continental Shelf Research* **28**(2): 309–317.

Thorne PD, Hurther D. 2014. An overview on the use of backscattered sound for measuring suspended particle size and concentration

profiles in non-cohesive inorganic sediment transport studies. *Continental Shelf Research* **73**: 97–118.

Topping DJ, Wright SA, Melis TS, Rubin DM. 2007. High-resolution measurements of suspended-sediment concentration and grain size in the Colorado River in Grand Canyon using a multi-frequency acoustic system. In Proceedings, 10th International Symposium on River Sedimentation. August 1–4, Moscow, Russia.

Topping DJ, Wright SA. 2016. *Long-term Continuous Acoustical Suspended-sediment Measurements in Rivers—Theory, Application, Bias, and Error*, US Geological Survey Professional Paper 1823. US Geological Survey: Reston, VA 98 pp. https://doi.org/10.3133/pp1823.

Turnipseed DP, Sauer VB. 2010. Discharge measurements at gaging stations. In *US Geological Survey Techniques and Methods*, Vol. **3-A8**. US Geological Survey: Reston, VA 87 pp.

Trevethan M, Martinelli A, Oliveira M, Ianniruberto M, Gualtieri C. 2015. Fluid mechanics, sediment transport and mixing about the confluence of Negro and Solimões Rivers, Manaus, Brazil. *E-Proceedings of the 36th IAHR World Congress*, 28 June–3 July, The Hague; the Netherlands, 12 pp.

Urick RJ. 1983. *Principles of Underwater Sound*, 3rd edn. McGraw-Hill: New York; 444.

Venditti JG, Church M, Attard ME, Haught D. 2016. Use of ADCPs for suspended sediment transport monitoring: an empirical approach. *Water Resources Research* **52**(4): 2715–2736. https://doi.org/10.1002/2015WR017348.

Vincent CE, MacDonald IT. 2015. A flocculi model for the acoustic scattering from flocs. *Continental Shelf Research* **104**: 15–24.

Wall GR, Nystrom EA, Litten S. 2006. *Use of an ADCP to Compute Suspended-sediment Discharge in the Tidal Hudson River, New York*, US Geological Survey Scientific Investigations Report 2006-5055. Us Geological Survey: Reston, VA 16 pp.

Wright SA, Topping DJ, Williams CA. 2010. Discriminating silt-and-clay from suspended-sand in rivers using sidelooking acoustic profilers. *Proceedings of the Joint Federal Interagency Conference on Sedimentation and Hydrologic Modeling*, June 27–July 1, Riviera Hotel, Las Vegas, NV. https://acwi.gov/sos/pubs/2ndJFIC/Contents/2C_Wright_03_01_10_paper.pdf